

One-dimensionality signature in optical conductivity of heavy-fermion CeIr₃B₂Bo Gyu Jang ¹, Kenneth R. O’Neal,² Christopher Lane,^{1,2} Thomas U. Böhm ³, Nicholas Sirica ², Dmitry Yarotski,² Eric D. Bauer,⁴ Filip Ronning,³ Rohit Prasankumar,² and Jian-Xin Zhu ^{1,2,*}¹Theoretical Division, Los Alamos National Laboratory, Los Alamos, New Mexico 87545, USA²Center for Integrated Nanotechnologies, Los Alamos National Laboratory, Los Alamos, New Mexico 87545, USA³Institute for Materials Science, Los Alamos National Laboratory, Los Alamos, New Mexico 87545, USA⁴Materials Physics and Application Division, Los Alamos National Laboratory, Los Alamos, New Mexico 87545, USA

(Received 6 February 2023; revised 12 April 2023; accepted 25 April 2023; published 9 May 2023)

In low dimensions, the combined effects of interactions and quantum fluctuations can lead to dramatically new physics distinct from that existing in higher dimensions. Here, we investigate the electronic and optical properties of CeIr₃B₂, a quasioone-dimensional (1D) Kondo lattice system, using *ab initio* calculations. The Ce atoms in the hexagonal crystal structure form 1D chains along the *c* axis, with extremely short Ce-Ce distances. The quasi-1D nature of the crystal structure is well reflected in its electronic structure. Extremely flat bands emerge within the *ab* plane of the Brillouin zone, yielding sharp optical transitions in the corresponding optical conductivity. Our calculations indicate that these prominent peaks in the optical conductivity provide a clear signature of quasi-1D heavy fermion systems.

DOI: [10.1103/PhysRevB.107.205116](https://doi.org/10.1103/PhysRevB.107.205116)**I. INTRODUCTION**

Heavy-fermion systems often exhibit a rich phase diagram, including magnetism, non-Fermi liquid physics, and unconventional superconductivity. The ground state of these materials is mainly governed by two major competing energy scales, the Ruderman-Kittel-Kasuya-Yoshida (RKKY) interaction and the Kondo interaction. A quantum phase transition occurs when the long-range RKKY interaction and the onsite Kondo interaction cancel each other, as one tunes external parameters such as pressure or magnetic field. If the quantum fluctuation driven transition is continuous, a quantum critical point (QCP) can be realized. In the vicinity of a QCP, exotic phenomena can be observed such as non-Fermi liquid behavior and superconductivity.

Low dimensionality enriches the anomalous behaviors of heavy-fermion systems and often modifies the critical behavior near the QCP. Near the pressure-induced quantum phase transition in three-dimensional (3D) bulk CeIn₃, the resistivity follows $\rho = \rho_0 + AT^\alpha$, where $\alpha \sim 1.6$ deviates from Fermi liquid behavior ($\alpha = 2$) [1,2]. On the other hand, *T*-linear resistivity behavior is observed near the quantum phase transition induced by dimensionality tuning in CeIn₃/LaIn₃ superlattices [3]. In addition to the dimensionality control in superlattices, there have been efforts to find low-dimensional heavy fermion materials. Quasitwo-dimensional (2D) heavy-fermion systems have been intensively studied, such as YbRh₂Si₂, Ce122 (e.g., CeCu₂Si₂), Ce115 (e.g., CeCoIn₅), and Ce218 (e.g., Ce₂CoIn₈). The resistivity behavior of CeCoIn₅ [4] and YbRh₂Si₂ [5,6] near the QCP is consistent with scattering from 2D antiferromagnetic fluctuations

[7]. Also the exotic quantum criticality in CeCu_{6-x}Au_x is related to strong magnetic two-dimensional quantum fluctuations [8–10]. 1T/1H-TaSe₂ heterostructures, tri-layer twisted graphene, and transition metal dichalcogenide (TMD) moiré materials have been suggested as artificial heavy-fermion systems without *f* electrons [11–15]. Recently, CeSiI has been proposed to be an intrinsic vdW 2D heavy-fermion material [16].

There are also a few reports of quasi-1D heavy-fermion systems, such as YbNi₄P₂ [17,18], CeCo₂Ga₈ [19], and CeM₃A₂ (*M* = Co, Rh, Ir/*A* = B, Si) [20–26]. Among them, CeM₃B₂ has received attention due to its abnormal properties. In this material, Ce atoms form 1D chains along the *c* axis as shown in Fig. 1. The Ce-Ce distance along the chain is much shorter than the Hill limit (~ 3.5 Å) and that of α -Ce (3.41 Å), which shows Pauli-like susceptibility [27]. In addition, CeRh₃B₂ and CeIr₃B₂ exhibit ferromagnetic ordering, while most Ce-based heavy-fermion materials order antiferromagnetically. CeRh₃B₂ has the highest magnetic ordering temperature among Ce-based materials (*T_C* = 115 K) and is followed by CeIr₃B₂ (*T_C* = 41 K) [24,26].

In this study, we elucidate the electronic and optical properties of the quasi-1D heavy-fermion material, CeIr₃B₂ using *ab initio* calculations. Due to the quasi-1D nature of the crystal structure, extremely flat band features occur in the *xy* plane. The resulting optical transitions between these flat bands yield notable peak structures in the optical conductivity, which are not observed in other heavy fermion materials with higher dimensionality.

II. COMPUTATIONAL METHOD

Density functional theory (DFT) calculations were performed using the WIEN2k code, which uses a full

*jxzhou@lanl.gov

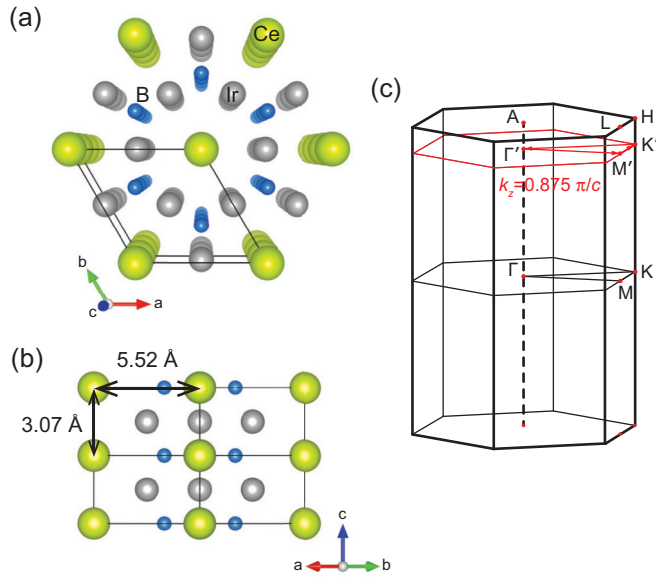


FIG. 1. Crystal structure of CeIr_3B_2 is shown in (a) a top view and (b) a side view. Green, gray, and blue indicate Ce, Ir, and B atoms, respectively. (c) The Brillouin zone of CeIr_3B_2 . A k_z path on the $k_z = 0.875\pi/c$ plane (red) is used for the band structure in Fig. 3.

potential linearized augmented plane-wave+local orbitals (L/APW+lo) method [28]. The Perdew-Burke-Ernzerhof generalized gradient approximation (PBE-GGA) was employed for the exchange-correlation potential [29]. Spin-orbit coupling (SOC) was considered to describe the relativistic effect of heavy Ce and Ir atoms. A $10 \times 10 \times 16$ k -point mesh was used for self-consistent calculation.

To study the correlation effect of Ce 4*f* electrons, we employed fully charge self-consistent dynamical mean-field theory calculations combined with DFT (DFT + DMFT) as implemented in DFT+Embedded DMFT (eDMFT) functional code [30]. A hybridization window from -10 eV to 10 eV with respect to the Fermi level (E_F) was used, along with the Hubbard parameters $U = 4$ eV, 5 eV, and 6 eV, and $J = 0.7$ eV. The rotational invariant Slater form of Coulomb interaction was used in the calculation. The impurity model was solved using a continuous time quantum Monte Carlo (CTQMC) solver [31]. The nominal double counting method was used, where the nominal occupancy of the Ce atom was set to one. More detailed information on DFT + DMFT calculation can be found in the Supplemental Material [32].

III. RESULTS

Figure 1 shows the crystal structure of CeIr_3B_2 in the high temperature hexagonal $p6/mmm$ phase. Below 395 K, the hexagonal crystal lattice slightly distorts, precipitating a structural phase transition to a monoclinic phase [24]. However, the difference between two structures is negligible so the hexagonal structure is used throughout this study for simplicity. In the pristine crystal, Ce atoms form quasi-1D chains along the c axis with a Ce-Ce intrachain distance of 3.07 Å and interchain distance of 5.52 Å. Ir atoms are located in the interstitial between the Ce chains facilitating weak interchain hopping within the ab plane. Furthermore, Ir-Ir distances along the c

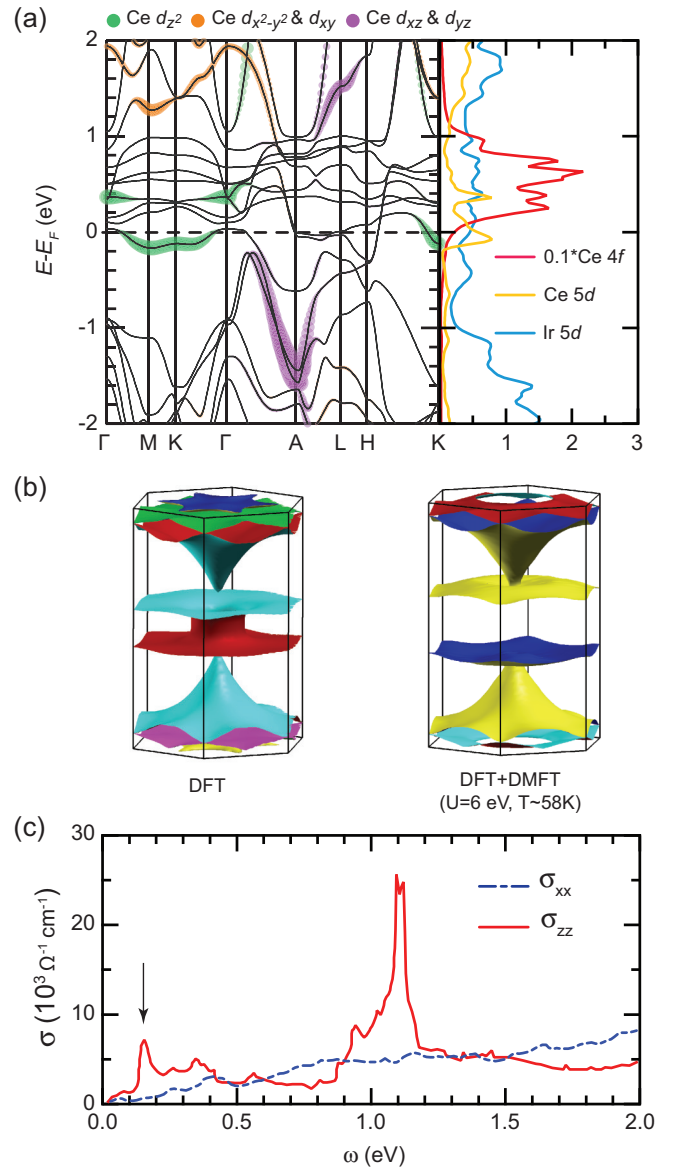


FIG. 2. (a) Electronic structure of CeIr_3B_2 obtained from DFT calculations. The size of green, orange, and purple dots are proportional to the Ce d_{z^2} , Ce $d_{x^2-y^2}$ & d_{xy} , and Ce d_{xz} & d_{yz} contribution, respectively. Red, yellow, and blue in right panel indicate Ce 4*f*, Ce 5*d*, and Ir 5*d* partial densities of states (PDOS), respectively. Here, the Ce 4*f* PDOS is divided by 10 for better comparison. (b) Calculated Fermi surfaces of CeIr_3B_2 . (c) Directional optical conductivity of CeIr_3B_2 obtained from DFT.

axis (3.07 Å) and in the ab plane (2.76 Å) are comparable such that the Ir atoms form an effective 3D network, in contrast to the Ce atoms. Figure 2(a) shows the DFT electronic band structure. Bands along k_z (See Γ -A and H-K paths) are more dispersive as compared to those in the plane as a result of the quasi-1D nature of the crystal structure. Concomitantly, the flat band dispersions of Ce 5*d* orbitals (mainly d_{z^2}) within the xy plane induce a sharp peak near the Fermi level (E_F) in the partial density of states (PDOS). On the other hand, the Ir 5*d* PDOS does not display any peak structure due to the comparable bonding distances along the c and in-plane

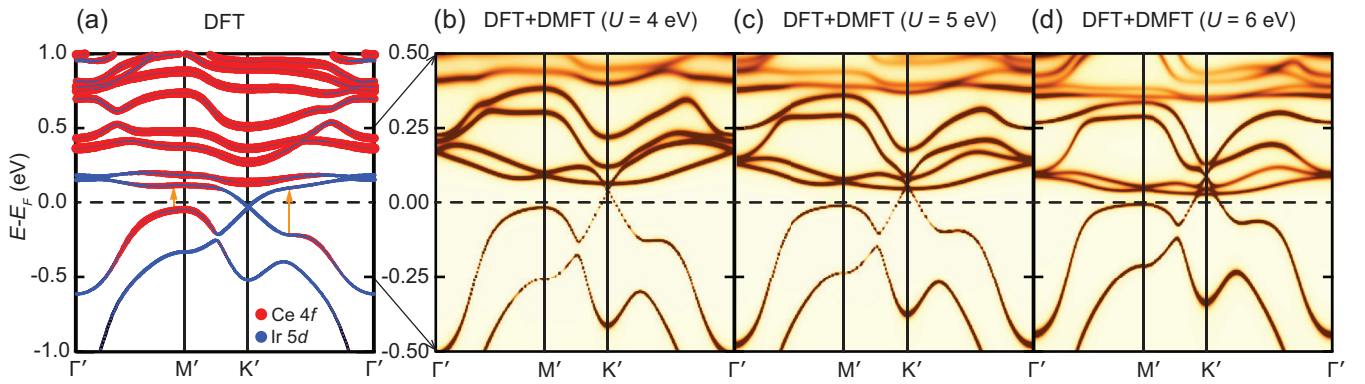


FIG. 3. Spectral function of CeIr_3B_2 on the $k_z = 0.875\pi/c$ plane obtained from (a) DFT and (b)–(d) DFT + DMFT ($T=58$ K). The k path used in the calculation is shown in Fig. 1(c). The possible optical transitions are shown with orange arrows in Fig. 3(a). As the U value increases, the hybridization gap around the M' and K' point becomes smaller.

directions. Moreover, due to the crystal structure geometry, Ce $4f$ orbitals are found to strongly hybridize with Ce $5d$ orbitals along the c axis, whereas Ce $4f$ states couple to Ir $5d$ orbitals within the ab plane. Although the Ce d_{z^2} orbital has a substantial contribution near the Fermi level on the Γ plane (xy plane with $k_z = 0$) and is coupled to Ce $4f$ $[5/2, \pm 1/2]$ state (See Fig. 1 in the Supplemental Material [32]), its contribution becomes smaller and the Ir d orbital contribution becomes important within the xy plane with finite k_z as shown in Fig. 3(a).

The calculated Fermi surfaces also demonstrate the quasi-1D nature of CeIr_3B_2 . Although the Fermi surface sheet originating from Ir $5d$ orbitals follows a dispersing cone-shaped surface, other Fermi surfaces clearly exhibit 1D characteristics, with flattening occurring along the xy direction. When the correlation effect of Ce $4f$ orbitals is treated properly in DFT + DMFT calculations, this quasi-1D nature is enhanced. In particular, the cylinder-shaped 2D-like Fermi surface near Γ point disappears in DFT + DMFT calculations.

Figure 2(c) presents the associated optical conductivity obtained from the DFT bands. While the in-plane optical conductivity (σ_{xx}) monotonically increases with energy, a notable peak structure is observed along the z axis (σ_{zz}). Specifically, a strong sharp peak is observed around 0.15 eV, as indicated by the black arrow. The energy scale of this optical transition is quite small, suggesting the Ce $4f$ orbitals participate in the optical transition. This kind of prominent peak is not observed in the quasi-2D heavy fermion materials at low-energy scales [33,34] (see also Fig. 3 in the Supplemental Material [32]).

To understand the origin of this optical transition, we analyzed the momentum resolved optical matrix elements (See Fig. 4 in the Supplemental Material [32]). When optical transitions are restricted to a small energy window of from 120 meV to 180 meV, the nonzero matrix elements are centered on the $(\frac{1}{3}, \frac{1}{3}, k_z)$ and $(0.5, 0.5, k_z)$ momentum points in the Brillouin zone, where k_z spans -0.5 to 0.5 . Furthermore, by scanning through the various values of k_z , the electronic bands responsible for the 150 meV optical transition are found to lie within the $k_z = 0.875\pi/c$ plane.

Figure 3 shows the band structure along the high-symmetry path in the $k_z = 0.875\pi/c$ plane [shown in red in Fig. 1(c)]. The size of blue and red dots are proportional to the Ir $5d$ and Ce $4f$ orbital weight, respectively. The contribution from Ce $5d$ orbitals was found to be negligible along this k path. Extremely flat band features now clearly dominate the low-energy spectrum near the Fermi level, thus revealing the underlying quasi-1D nature of CeIr_3B_2 . The possible optical transitions are shown with orange arrows in Fig. 3(a). Near M' , a hybridization gap of ~ 150 meV is observed, consistent with the sharp peak in σ_{zz} . Due to the mixture of orbital character at M' , both Ir $5d$ and Ce $4f$ states are found to be involved in the optical transition. Furthermore, the weak peak at ~ 0.35 eV in σ_{zz} can be attributed to the transition occurring between K' and Γ' . Overall, we find the strong sharp peaks in the optical conductivity can be regarded as a clear signature of a quasi-1D heavy-fermion system.

Next, we performed DFT + DMFT calculations with varying Coulomb interaction U values to investigate the effect of electronic correlations on the Ce $4f$ orbitals [Figs. 3(b)–3(d)]. Because of the strong renormalization in DFT + DMFT calculations, a small energy window is used for a better comparison to the DFT calculation in Fig. 3(a). The mass enhancement (m^*/m) estimated from the self-energy varies from 2 to 4.6 depending on the U value ($m^*/m = 1 - \partial \text{Im}\Sigma(i\omega)/\partial \omega|_{\omega \rightarrow 0^+}$). The relatively small mass enhancement compared to other typical heavy-fermion systems suggests the presence of strong $f-c$ hybridization and the high Kondo temperature scale of CeIr_3B_2 . Not only the bandwidth of Ce $4f$ bands, but the hybridization gap also becomes smaller as U value increases. The hybridization gap near the M' point in the $U = 6$ eV calculation is ~ 75 meV, which is almost half the size of DFT calculations.

Figure 4(a) shows the DFT + DMFT ($U=6$ eV) total optical conductivity, including the Drude contribution, for varying temperature values ($T = 58$ K, 116 K, and 290 K). The Drude peak is quite prominent in σ_{zz} , but is very weak in σ_{xx} . These features clearly reveal the quasi-1D nature of CeIr_3B_2 . The anisotropic behavior of the optical conductivity is related to the anisotropic properties of effective band mass or group velocity in this system.

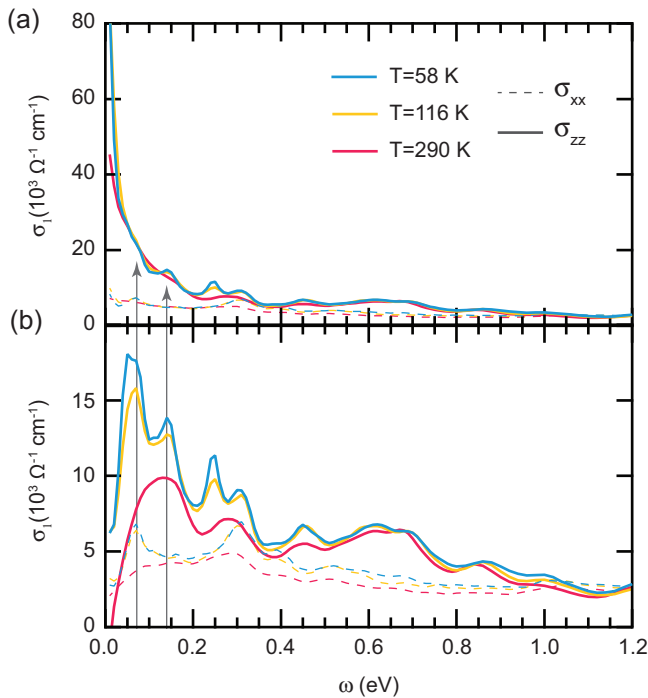


FIG. 4. Frequency-dependent optical conductivity (a) with and (b) without the Drude peak calculated within DFT + DMFT ($U = 6$ eV) for varying temperature values ($T = 58$ K, 116 K, and 290 K).

As the temperature increases, the Drude peak decreases in intensity. Despite this, a clear sharp Drude peak persists even up to 290 K, indicating a high Kondo temperature scale in CeIr_3B_2 [24,26]. For comparison, the resistivity of CeCoIn_5 gradually increases below ~ 200 K, which can be defined experimentally as the onset temperature of the Kondo effect [35,36]. Although it is difficult to define the Kondo energy scale of CeIr_3B_2 from resistivity data due to the structural transition, the resistivity of CeIr_3B_2 already starts to increase immediately below the structural phase transition temperature of 395 K. However, the short Ce-Ce distance along the c axis is robust against the structural phase transition. This indicates that the extremely short Ce-Ce distance along the chain is responsible for the high Kondo temperature of this material. The tensile strain along the c direction would be interesting to understand its high Kondo temperature scale.

Figure 4(b) shows the optical conductivity without the Drude part (only interband transitions). Because of the hybridization gap renormalization discussed in Fig. 3, the sharp peak observed in the DFT optical calculations has shifted to ~ 75 meV. Another notable peak is observed at ~ 0.13 eV, which corresponds to the optical transition occurring between K' and Γ' [see orange arrows in Fig. 3(a)]. Flat bands originating from the quasi-1D nature become even more flattened due to the strong mass renormalization, resulting in the enhanced optical transitions (See Fig. 5 in the Supplemental Material [32]). Although the Drude part from the intraband transitions is quite strong, due to the short Ce-Ce distance along the c direction, these notable peaks arising from interband transitions are still noticeable in the total optical conductivity.

There is a subtle difference between the temperature dependence of the two notable peaks. As the temperature increases, the peak at 75 meV diminishes more rapidly compared to the peak at 0.13 eV. The flat valence band near M' moves upward and becomes incoherent, making the optical transition ill-defined (See Fig. 6 in the Supplemental Material [32]). However, the hybridization gap between K' and Γ' is clearly defined even at 290 K. As a result, the optical transition originating from the hybridization gap between K' and Γ' yields the most prominent peak at 290 K.

One remark is in order, since the DFT + DMFT conductivity is calculated within a single-site DMFT framework, which is a good approximation for typical 3D systems, the vertex correction is not included in the present work. Nevertheless, we do not anticipate that the inclusion of vertex corrections will completely change our observation, though it can modify the energy scale or the intensity. First, although the system has quasi-1D structure when we only focus on Ce atoms, the local environment of Ce atoms remains 3D-like, surrounded by Ir and B atoms. Second, the effect of the vertex correction is usually small in many materials [37]. In addition, the study on 2D Hubbard models on a square lattice has demonstrated that vertex corrections mainly contribute to the optical conductivity at the scale of the Coulomb repulsion U and are less important at low frequency [38]. A recent study shows a similar result, that the position of high frequency peak at $\sim U$ is affected by the inclusion of the vertex correction [39]. The same study has also observed that the Drude peak becomes more coherent (a larger weight and a narrower width) in the presence of the vertex correction. The similar behavior has also been obtained in a triangular lattice Hubbard model but the effect is less significant than on the 2D square lattice [40]. Therefore, the prominent peak in the optical conductivity would be robust even in the presence of the vertex correction.

IV. SUMMARY

In summary, we have observed a prominent optical transition peak at low-energy scales in the quasi-1D heavy-fermion system CeIr_3B_2 . This kind of strong sharp peak cannot be found in heavy-fermion materials with higher dimensionality. The transitions between the extremely flat bands originating from the quasi-1D Ce chains result in sharp peaks in the optical conductivity. This notable peak is robust in DFT + DMFT calculations, albeit shifted to a lower energy scale due to the strong mass renormalization. Therefore, this prominent peak feature can be regarded as a clear signature of quasi-1D heavy-fermion systems.

ACKNOWLEDGMENTS

We thank Hongchul Choi and Chao Cao for helpful discussions. Work at Los Alamos was carried out under the auspices of the U.S. Department of Energy (DOE) National Nuclear Security Administration (NNSA) under Contract No. 89233218CNA000001. It was supported by the LANL LDRD Program, UC Laboratory Fees Research Program (Grant No. FR-20-653926), and in part by the Center for Integrated Nanotechnologies, a DOE BES user facility, in partnership with

the LANL Institutional Computing Program for computational resources. E.D.B. acknowledges support from the U.S.

DOE BES Materials Sciences and Engineering Division under the “Quantum Fluctuations in Narrow Band Systems” project.

- [1] N. Mathur, F. Grosche, S. Julian, I. Walker, D. Freye, R. Haselwimmer, and G. Lonzarich, Magnetically mediated superconductivity in heavy fermion compounds, *Nature (London)* **394**, 39 (1998).
- [2] G. Knebel, D. Braithwaite, P. C. Canfield, G. Lapertot, and J. Flouquet, Electronic properties of CeIn₃ under high pressure near the quantum critical point, *Phys. Rev. B* **65**, 024425 (2001).
- [3] H. Shishido, T. Shibauchi, K. Yasu, T. Kato, H. Kontani, T. Terashima, and Y. Matsuda, Tuning the dimensionality of the heavy fermion compound CeIn₃, *Science* **327**, 980 (2010).
- [4] A. Malinowski, M. F. Hundley, C. Capan, F. Ronning, R. Movshovich, N. O. Moreno, J. L. Sarrao, and J. D. Thompson, *c*-axis magnetotransport in CeCoIn₅, *Phys. Rev. B* **72**, 184506 (2005).
- [5] S. Friedemann, T. Westerkamp, M. Brando, N. Oeschler, S. Wirth, P. Gegenwart, C. Krellner, C. Geibel, and F. Steglich, Detaching the antiferromagnetic quantum critical point from the Fermi-surface reconstruction in YbRh₂Si₂, *Nat. Phys.* **5**, 465 (2009).
- [6] D. Nguyen, A. Sidorenko, M. Taupin, G. Knebel, G. Lapertot, E. Schubert, and S. Paschen, Superconductivity in an extreme strange metal, *Nat. Commun.* **12**, 4341 (2021).
- [7] T. Moriya and K. Ueda, Spin fluctuations and high temperature superconductivity, *Adv. Phys.* **49**, 555 (2000).
- [8] A. Rosch, A. Schröder, O. Stockert, and H. v. Löhneysen, Mechanism for the Non-Fermi-Liquid Behavior in CeCu_{6-x}Au_x, *Phys. Rev. Lett.* **79**, 159 (1997).
- [9] J.-X. Zhu, D. R. Grempel, and Q. Si, Continuous Quantum Phase Transition in a Kondo Lattice Model, *Phys. Rev. Lett.* **91**, 156404 (2003).
- [10] J.-X. Zhu, S. Kirchner, R. Bulla, and Q. Si, Zero-Temperature Magnetic Transition in an Easy-Axis Kondo Lattice Model, *Phys. Rev. Lett.* **99**, 227204 (2007).
- [11] V. Vaño, M. Amini, S. C. Ganguli, G. Chen, J. L. Lado, S. Kezilebieke, and P. Liljeroth, Artificial heavy fermions in a van der Waals heterostructure, *Nature (London)* **599**, 582 (2021).
- [12] W. Ruan, Y. Chen, S. Tang, J. Hwang, H.-Z. Tsai, R. L. Lee, M. Wu, H. Ryu, S. Kahn, F. Liou, C. Jia, A. Aikawa, C. Hwang, F. Wang, Y. Choi, S. G. Louie, P. A. Lee, Z.-X. Shen, S.-K. Mo, and M. F. Crommie, Evidence for quantum spin liquid behaviour in single-layer 1T-TaSe₂ from scanning tunnelling microscopy, *Nat. Phys.* **17**, 1154 (2021).
- [13] A. Ramires and J. L. Lado, Emulating Heavy Fermions in Twisted Trilayer Graphene, *Phys. Rev. Lett.* **127**, 026401 (2021).
- [14] A. Kumar, N. C. Hu, A. H. MacDonald, and A. C. Potter, Gate-tunable heavy fermion quantum criticality in a moiré kondo lattice, *Phys. Rev. B* **106**, L041116 (2022).
- [15] D. Guerci, J. Wang, J. Zang, J. Cano, J. Pixley, and A. Millis, Chiral kondo lattice in doped MoTe₂/WSe₂ bilayers, *Sci. Adv.* **9**, eade7701 (2023).
- [16] B. G. Jang, C. Lee, J.-X. Zhu, and J. H. Shim, Exploring two-dimensional van der Waals heavy-fermion material: Data mining theoretical approach, *npj 2D Mater. Appl.* **6**, 80 (2022).
- [17] C. Krellner, S. Lausberg, A. Steppke, M. Brando, L. Pedrero, H. Pfau, S. Tencé, H. Rosner, F. Steglich, and C. Geibel, Ferromagnetic quantum criticality in the quasi-one-dimensional heavy fermion metal YbNi₄P₂, *New J. Phys.* **13**, 103014 (2011).
- [18] A. Steppke, R. KÜchler, S. Lausberg, E. Lengyel, L. Steinke, R. Borth, T. Lühmann, C. Krellner, M. Nicklas, C. Geibel, F. Steglich, and M. Brando, Ferromagnetic quantum critical point in the heavy-fermion metal YbNi₄(P_{1-x}As_x)₂, *Science* **339**, 933 (2013).
- [19] L. Wang, Z. Fu, J. Sun, M. Liu, W. Yi, C. Yi, Y. Luo, Y. Dai, G. Liu, Y. Matsushita, K. Yamaura, L. Lu, J.-G. Cheng, Y. feng Yang, Y. Shi, and J. Luo, Heavy fermion behavior in the quasi-one-dimensional Kondo lattice CeCo₂Ga₈, *npj Quantum Mater.* **2**, 36 (2017).
- [20] Y. Muro, Y. Ohno, T. Okada, and K. Motoya, Multi-step metamagnetism in CeIr₃Si₂, *J. Magn. Magn. Mater.* **310**, 389 (2007).
- [21] K. Shigetoh, A. Ishida, Y. Ayabe, T. Onimaru, K. Umeo, Y. Muro, K. Motoya, M. Sera, and T. Takabatake, Easy-plane magnetocrystalline anisotropy in the multistep metamagnet CeIr₃Si₂, *Phys. Rev. B* **76**, 184429 (2007).
- [22] D. Kaczorowski and T. Komatsubara, Complex magnetic behavior in single-crystalline CeRh₃Si₂, *Physica B: Condens. Mater.* **403**, 1362 (2008).
- [23] A. P. Pikul, D. Kaczorowski, Z. Gajek, J. Stępień Damm, A. Ślebarski, M. Werwiński, and A. Szajek, Giant crystal-electric-field effect and complex magnetic behavior in single-crystalline CeRh₃Si₂, *Phys. Rev. B* **81**, 174408 (2010).
- [24] K. Kubota, E. Matsuoka, Y. Funasako, T. Mochida, T. Sakurai, H. Ohta, T. Onimaru, T. Takabatake, and H. Sugawara, Weak ferromagnetism below 41 K and structural transition at 395 K in CeIr₃B₂ single crystal, *J. Phys. Soc. Jpn.* **82**, 104715 (2013).
- [25] A. Amorese, D. Khalyavin, K. Kummer, N. B. Brookes, C. Ritter, O. Zaharko, C. B. Larsen, O. Pavlosiuk, A. P. Pikul, D. Kaczorowski, M. Gutmann, A. T. Boothroyd, A. Severing, and D. T. Adroja, Metamagnetism and crystal-field splitting in pseudo-hexagonal CeRh₃Si₂, *Phys. Rev. B* **105**, 125119 (2022).
- [26] A. Amorese, P. Hansmann, A. Marino, P. Körner, T. Willers, A. Walters, K.-J. Zhou, K. Kummer, N. B. Brookes, H.-J. Lin, C.-T. Chen, P. Lejay, M. W. Haverkort, L. H. Tjeng, and A. Severing, Orbital selective coupling in CeRh₃B₂: Coexistence of high curie and high kondo temperatures, *Phys. Rev. B* **107**, 115164 (2023).
- [27] J. Kim, D. C. Ryu, C. J. Kang, K. Kim, H. Choi, T. S. Nam, and B. I. Min, Topological phase transition in the archetypal *f*-electron correlated system of cerium, *Phys. Rev. B* **100**, 195138 (2019).
- [28] P. Blaha, K. Schwarz, F. Tran, R. Laskowski, G. K. H. Madsen, and L. D. Marks, WIEN2k: An APW+lo program for calculating the properties of solids, *J. Chem. Phys.* **152**, 074101 (2020).
- [29] J. P. Perdew, K. Burke, and M. Ernzerhof, Generalized Gradient Approximation Made Simple, *Phys. Rev. Lett.* **77**, 3865 (1996).
- [30] K. Haule, C.-H. Yee, and K. Kim, Dynamical mean-field theory within the full-potential methods: Electronic structure of

- CeIrIn₅, CeCoIn₅, and CeRhIn₅, *Phys. Rev. B* **81**, 195107 (2010).
- [31] K. Haule, Quantum Monte Carlo impurity solver for cluster dynamical mean-field theory and electronic structure calculations with adjustable cluster base, *Phys. Rev. B* **75**, 155113 (2007).
- [32] See Supplemental Material at <http://link.aps.org/supplemental/10.1103/PhysRevB.107.205116> for the crystal electric field splitting and temperature scales of CeIr₃B₂, the comparison between fully charge self-consistent calculation and non charge self-consistent calculation, the optical conductivity of representative quasi-2D heavy fermion materials, the optical transition k -distribution in the reciprocal space, the optical conductivity depending on U values, the temperature dependent spectral function obtained from DFT+DMFT with $U=6$ eV.
- [33] E. J. Singley, D. N. Basov, E. D. Bauer, and M. B. Maple, Optical conductivity of the heavy fermion superconductor CeCoIn₅, *Phys. Rev. B* **65**, 161101(R) (2002).
- [34] B. G. Jang, B. Goh, J. Kim, J. N. Kim, H. Kang, K. Haule, G. Kotliar, H. Choi, and J. H. Shim, Orbital anisotropy of heavy fermion Ce₂IrIn₈ under crystalline electric field and its energy scale, *Phys. Rev. B* **105**, 115147 (2022).
- [35] S. Jang, J. D. Denlinger, J. W. Allen, V. S. Zapf, M. B. Maple, J. N. Kim, B. G. Jang, and J. H. Shim, Evolution of the Kondo lattice electronic structure above the transport coherence temperature, *Proc. Natl. Acad. Sci. USA* **117**, 23467 (2020).
- [36] M. Lee, Y.-S. Seo, S. Roh, S. Lee, J. Kim, J. Kim, T. Park, J. H. Shim, and J. Hwang, Temperature-dependent f -electron evolution in CeCoIn₅ via a comparative infrared study with LaCoIn₅, *Results Phys.* **47**, 106376 (2023).
- [37] D. N. Basov, R. D. Averitt, D. van der Marel, M. Dressel, and K. Haule, Electrodynamics of correlated electron materials, *Rev. Mod. Phys.* **83**, 471 (2011).
- [38] N. Lin, E. Gull, and A. J. Millis, Optical conductivity from cluster dynamical mean-field theory: Formalism and application to high-temperature superconductors, *Phys. Rev. B* **80**, 161105(R) (2009).
- [39] J. Vučičević, J. Kokalj, R. Žitko, N. Wentzell, D. Tanasković, and J. Mravlje, Conductivity in the Square Lattice Hubbard Model at High Temperatures: Importance of Vertex Corrections, *Phys. Rev. Lett.* **123**, 036601 (2019).
- [40] T. Sato, K. Hattori, and H. Tsunetsugu, Transport criticality in triangular lattice Hubbard model, *J. Phys. Soc. Jpn.* **81**, 083703 (2012).